frontiers in Marine Science

ORIGINAL RESEARCH
published: 10 October 2018
doi: 10.3389/fmars.2018.00363

Monitoring of Marine Biofilm Formation Dynamics at Submerged Solid Surfaces With Multitechnique Sensors

Maciej Grzegorczyk[1], *Stanisław Józef Pogorzelski*[1], *Aneta Pospiech*[2] *and Katarzyna Boniewicz-Szmyt*[3]*

[1] *Institute of Experimental Physics, Faculty of Mathematics, Physics and Informatics, University of Gdańsk, Gdańsk, Poland,* [2] *Institute of Geography, Faculty of Geography and Oceanography, University of Gdańsk, Gdańsk, Poland,* [3] *Department of Physics, Gdynia Maritime University, Gdynia, Poland*

OPEN ACCESS

Edited by:
Karol Kulinski,
Institute of Oceanology (PAN), Poland

Reviewed by:
Violetta Drozdowska,
Institute of Oceanology (PAN), Poland
Ian R. Jenkinson,
Chinese Academy of Sciences, China

***Correspondence:**
Katarzyna Boniewicz-Szmyt
kbon@am.gdynia.pl

Specialty section:
This article was submitted to Coastal Ocean Processes, a section of the journal Frontiers in Marine Science

Received: *16 April 2018*
Accepted: *20 September 2018*
Published: *10 October 2018*

Citation:
Grzegorczyk M, Pogorzelski SJ, Pospiech A and Boniewicz-Szmyt K (2018) Monitoring of Marine Biofilm Formation Dynamics at Submerged Solid Surfaces With Multitechnique Sensors. Front. Mar. Sci. 5:363. doi: 10.3389/fmars.2018.00363

Biofouling on artificial and biotic solid substrata was studied in several locations in near-shore waters of the Baltic Sea (Gulf of Gdansk) during a three-year period with contact angle wettability, confocal microscopy and photoacoustic spectroscopy techniques. As a reference, the trophic state of water body was determined from chemical analyses according to the following parameters: pH, dissolved O_2, phosphate, nitrite, nitrate, ammonium concentrations, and further correlated to the determined biofilm characterizing parameters by means of Spearman's rank correlation procedure. Biofilm adhesive surface properties (surface free energy, work of adhesion) were obtained with the contact angle hysteresis (CAH) approach using an automatic captive bubble solid surface wettability sensor assigned for *in-situ*, on-line, and quasi-continuous measurements of permanently submerged samples (Pogorzelski et al., 2013; Pogorzelski and Szczepanska, 2014). From confocal reflection microscopy (COCRM) data, characteristic biofilm structural signatures such as biovolume, substratum coverage fraction, area to volume ratio, spatial heterogeneity, mean thickness, and roughness) were determined at different stages of microbial colony development. Photosynthetic properties [photosynthetic energy storage (ES), photoacoustic amplitude and phase spectra] of biofilm communities exhibited a seasonal variation, as indicated by a novel closed-cell type photoacoustic spectroscopy (PAS) system. Mathematical modeling of a marine biofilm under steady state was undertaken with two adjustable parameters, of biological concern i.e., the specific growth rate and induction time, derived from simultaneous multitechnique signals. A set of the established biofilm structural and physical parameters could be modern water body trophic state indexes.

Keywords: baltic waters, submerged substrata biofilm, multitechnique biofilm parameters, biofilm growth model, trophic state indexes, marine bioassessment indicators

INTRODUCTION

Steps of biofilm formation are illustrated in **Figure 1A** (Rubio, 2002). The characteristic formation time scale is apparently related to the length scale of the organisms forming the biofilm colony on solid submersed surfaces (**Figure 1B**). The biofilm development at solid substrata in aquatic environments is presented as a sequence of phases starting from the formation of a conditioning film via microfouling to complex mature macrofouling organisms community. Various time scales for biofilm-related processes were found (Picioreanu et al., 1998). Periphyton is a complex mixture of algae, cyanobacteria, heterotrophic microbes, and detritus this is attached to submerged surfaces in most aquatic ecosystems (Dang and Lovell, 2016). Microbial substrata colonization leads to production of particular substances named extracellular polymeric substances (EPS) consisting of proteins, glycoproteins, glycolipids, extracellular DNA, polysaccharides etc. EPS is critical in the formation of microcolony aggregates acting as a binding hydrated and heterogeneous matrix or "glue" which holds microbes together, and bind them to the submersed substratum (Flemming, 2009). Periphyton serves as an indicator of water quality because:

- it has naturally high number of species;
- it has a fast response to changes;
- it is easy to sample;
- it is known for tolerance/sensitivity to change.

There are several factors affecting the marine biofilm adhesion, apart from the surface free energy of substrata (Zhao et al., 2005), like surface electricity, surface architecture, temperature, fluid shear stress or contact time (Thomas and Muirhead, 2009).

A short generation time, sessile nature and fast responsiveness to environmental conditions make biofilms being water chemistry bioindicators particularly suitable as a monitoring tool in Baltic Sea eutrophication studies. There are several methods used in biofilm formation studies, for a review see (Azeredo et al., 2017). The contact angle (CA) captive bubble technique (Pogorzelski et al., 2013, 2014) adapted here allows the outermost biofilm surface wettability evolution to be monitored quasi-continuously and *in-situ* at subsequent stages of the biofilm formation starting from the molecular adsorption phase (second-minute time scale) to the final mature stage of the marine biofilm cycle. Geometric, structural and biological, commonly evaluated biofilm characteristics like: biovolume, coverage fraction, area to volume ratio, spatial heterogeneity, number of species, mean thickness, roughness, fractal dimension in 2D etc. were on-line determined from confocal reflection microscopy (COCRM) data (Inaba et al., 2013), processed with graphical programs (COMSTAT, ImageJ, CMEIAS, PHLIP etc.). Biofilm is also a photosynthetic system containing a mixture of pigments (Schagerl and Donabaum, 2003).The photosynthetic properties (photosynthetic energy storage ES, photoacoustic amplitude, and phase spectra) of biofilm communities should reveal a seasonal variation, as studied here, by a novel closed-cell type photoacoustic spectroscopy (PAS) system (Szurkowski et al., 2001). The main aim of the work is to demonstrate a close correlation between the biofilm structural state derived from multitechnique physical sensors and the standard water body trophic state indicators on the basis of comprehensive measurements performed in near-shore shallow waters of the Baltic Sea (Gulf of Gdansk). The analyses established a several biological compounds composing the biofilm (bacteria, micro-algae and ConA-stained EPS), which demonstrated differentiated growth rate values evaluated with multi-sensor signals. The biofilm growth kinetics curve was approximated with Gompertz functions (Zwietering et al., 1990), where the specific growth rates μ_i and induction times λ_i where introduced from the simultaneous multi-technique data. Moreover, knowledge of three-dimensional structure of the biofilm and the distribution of species concerned is crucial in managing and preventing uncontrolled colonization of great practical value for undersea engineering constructions.

It should be pointed out that so many methods and several parameters were measured since the biofilm structure, composition, state of evolution, photosynthetic system features respond to environmental stresses in a very complex way. In addition, not all the selected quantities turned out to be sensitive enough in trophic state monitoring.

MATERIALS AND METHODS

Materials-Biofilm Sample Collection

Several artificial solid substrata (glass, metallic, polymeric) and biotic (wood, macrophytes) of varying surface energy placed in a transparent plastic loaded box were deployed at a depth of 0.5 m in near-shore waters of the southern Baltic Sea, for a certain time (**Figure 2A**).

The solid substrata had a form of rectangular plates (dimensions: $77 \times 26 \times 1.5$ mm) or disks (diameter $= 1.8$ mm, thickness $= 0.1$ mm) were mounted in a plastic holders oriented perpendicularly (**Figure 2B**). The artificial model substrata were cleaned by immersion in a methanol/chloroform mixture (1:2 v/v) and toluene; subsequently the samplers were dried before deployment (**Figure 2C**). Biofilm accumulation time was ranging from 1 to 24 days; probes were studied every month from May to November, 2016. Biofilm samples (5–10 from the particular location) together with the adjacent water were collected in a plastic bottle, not allowed to dry out, and further processed under laboratory conditions within an hour after collection. The submerged macrophyte (*Potamogeton lucens*) was also used as the model natural substrates. However, as a natural material, a large diversity in the surface morphology of the macrophyte leaf surface was reflected in a large variability of the particular parameter values measured. Biofilm wet weight (BWW) was chosen as a direct biofilm collection efficiency indicator of the studied samples (Simões et al., 2007), determined by weighting (microbalance; $\Delta m = \pm 10^{-4}$ g) a biofilm material scratched with a scalpel from the known film-covered area A (a few cm^2).

METHODS

Evaluations of Water Body Trophic State

For contact angle wettability studies, seawater samples were collected in near-shore coastal locations [at Gdansk, Sopot,

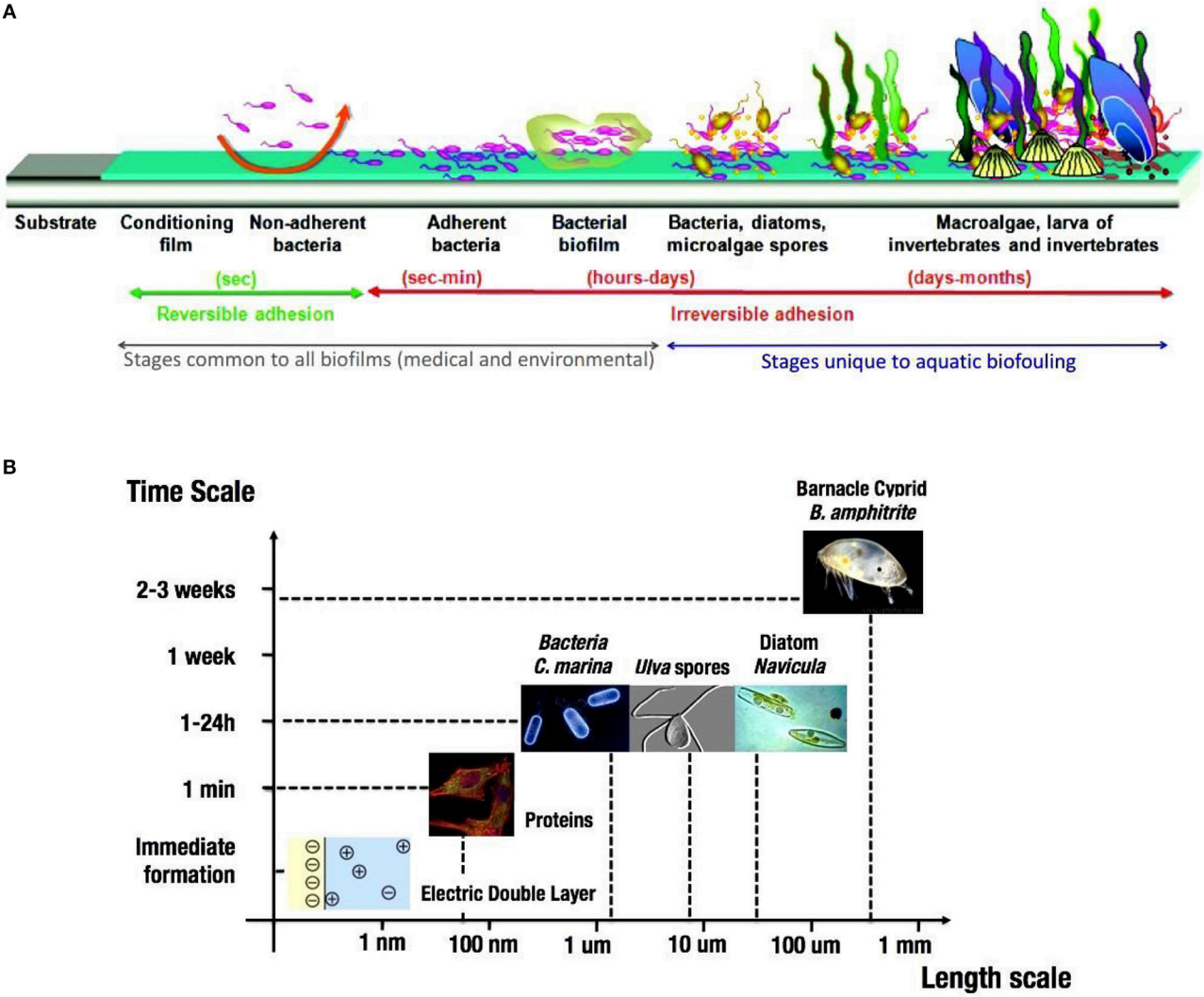

FIGURE 1 | (A) Stages of biofilm formation (modified after Rubio, 2002). **(B)** Characteristic time of biofilm formation vs. length scale of organism's colony (data taken from Dang and Lovell, 2016).

Gdynia (southern Baltic Sea)] had pH 8.2–8.6 ± 0.1 and surface tension γ_{LV} = 69.2–73.3 ± 0.1 mJ m^{-2} at 20°C, were used as the model water phase. The surface tension γ_{LV} was measured *in situ* with a Bubble Pressure Tensiometer BP2100 (PocketDyne, Krűss, Germany). A trophic status of the water body was determined according to the following parameters: pH, dissolved O_2, phosphate (PO_4^{3-}), nitrite (NO_2^-), nitrate (NO_3^-), ammonium (NH_4^+), and Secchi depth. The seawater chemical parameters were also taken from SatBałtyk System data base (available at http://satbaltyk.iopan.gda.pl). Average values of the trophic state indexes (TSI) were calculated according to Carlson (1977). Relationships between the physicochemical variables and the biofouled solid substrata wettability, geometric – morphological, and photoacoustic spectra parameters were analyzed by Spearman's rank correlation routine.

Contact Angle Captive Bubble Apparatus

The solid surface wettability, in particular the surface free energy, is commonly derived from static contact angle measurements by means of several theoretical approaches (Gindl et al., 2001).

In contrast, CA hysteresis (CAH= $\Theta_A - \Theta_R$) formalism developed by Chibowski (2003) allows the apparent surface free energy of the solid γ_{SV} to be determined, and is based on the three measurable quantities: the dynamic contact angles (advancing- Θ_A and receding- Θ_R), and the surface tension of the probe liquid γ_{LV}. The CA captive bubble experimental set-up together with the operational procedure was described in detail elsewhere (Pogorzelski et al., 2013, 2014). The gas bubble at the end of the micropipette touching the studied surface is compressed to determine Θ_R. In the next step, the bubble is drawn up and Θ_A was measured by means of ImageJ program applied to images taken by a side-situated camera (**Figures 3A,B**).

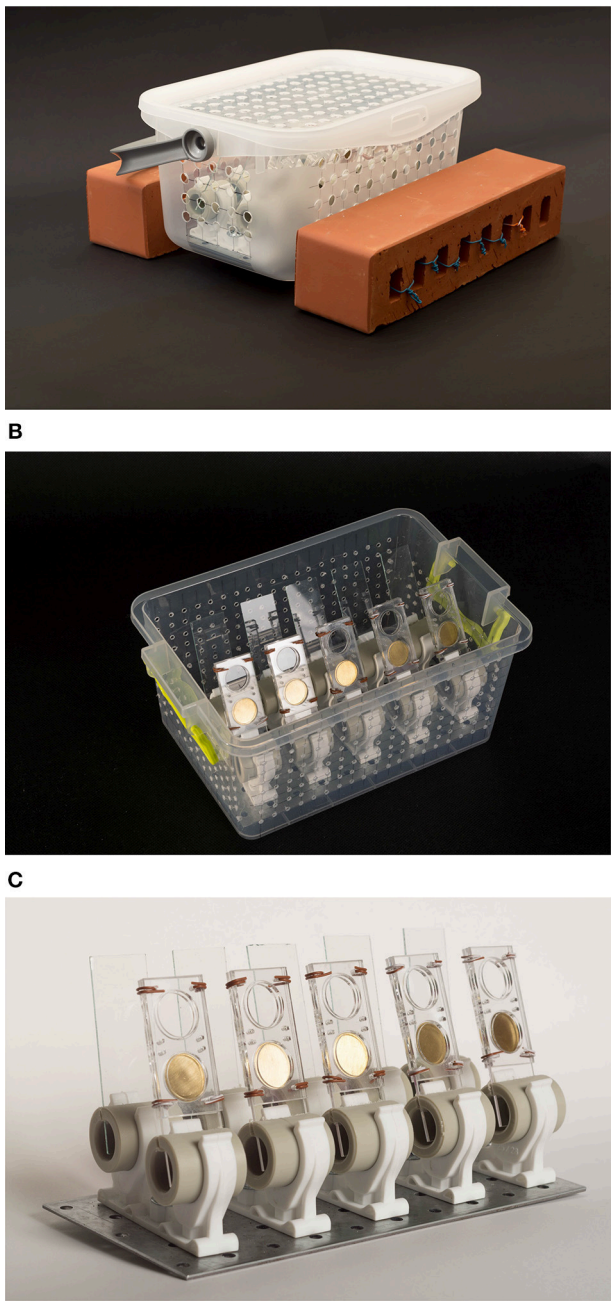

FIGURE 2 | Biofilm sampling devices: **(A)** loaded sampling substrata carrier ready to deployment; **(B)** perpendicularly-oriented rectangular plates or disks placed in a plastic box; **(C)** sampling substrata plastic holders.

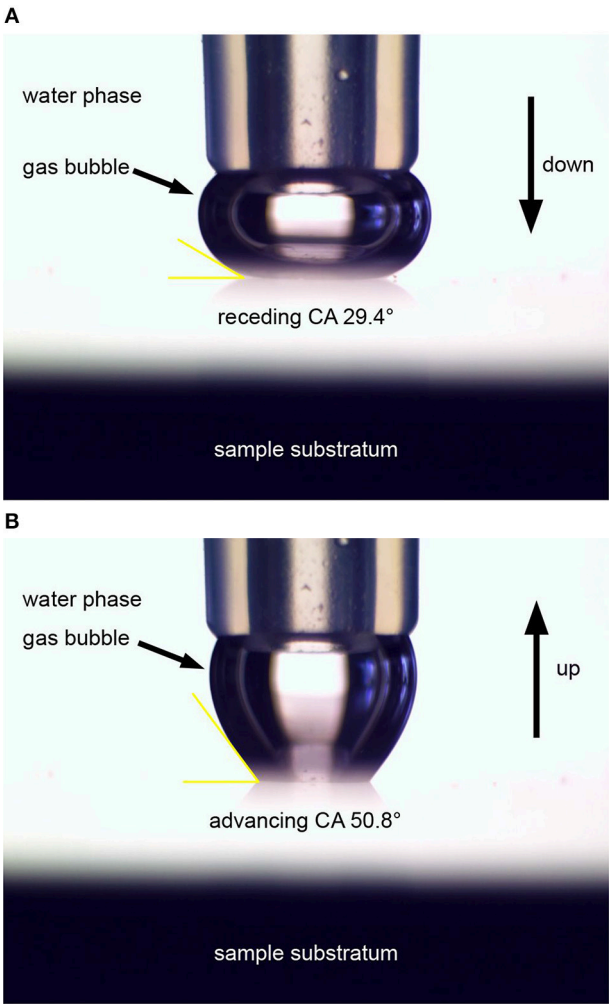

FIGURE 3 | Determination of dynamic CAs with a captive bubble technique for fully-hydrated biofouled surfaces: **(A)** receding CA; **(B)** advancing CA.

In these studies, the novel automated, computer-operated version of the system is shown in **Figure 4**. The outermost biofouled glass plate surface (4) is sensed with a gas bubble formed at the tip of a microsiringe, placed in a water tank (1). Captive bubble microsyringe set-up (2–3) is computer-controlled. The digital cameras (5) allow one to CA determination. A Long-axis microscope is used for selection the area to be studied (5–6). The surface wettability mapping is realized with a step motor + gear utility by positioning the sensing tip along x-y axes (7).

The peristaltic pump+tubes (8, 10) are used to control the water flow circulation in a measuring cell which is illuminated with a diffused light source.

The apparent solid surface free energy γ_{SV} and the remaining wettability parameters can be expressed with the following equations (Chibowski, 2003, 2007):

$$\text{Adsorbed matter 2D film pressure}: \Pi = \gamma_{LV}(\cos\Theta_R - \cos\Theta_A)$$

$$\text{Apparent surface energy}: \gamma_{SV} = \Pi(1+\cos\Theta_A)^2/[(1+\cos\Theta_R)^2 - (1+\cos\Theta_A)^2]$$

$$\text{Adhesion work}: W_A = \gamma_{LV}(1+\cos\Theta_A)$$

$$\text{Cohesion work}: W_C = 2\gamma_{LV}$$

$$\text{Spreading work}: W_S = W_A - W_C$$

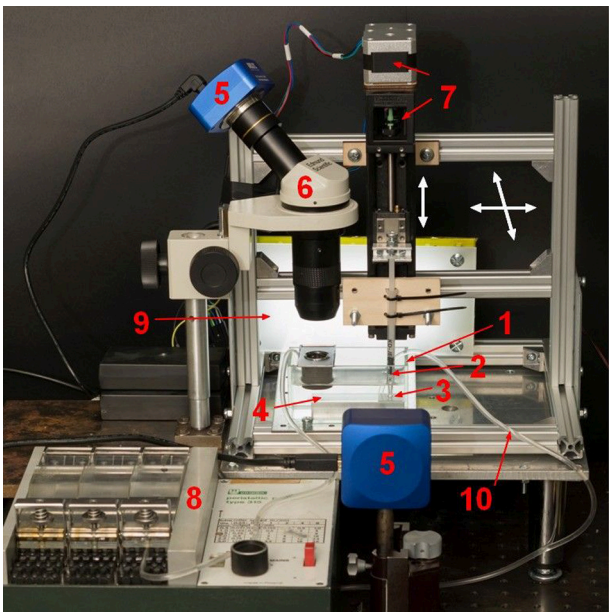

FIGURE 4 | Elements of the automatic, captive bubble CA determination system (for description see text).

where: Θ_A is the advancing contact angle, Θ_R - the receding contact angle, CAH = Θ_A- Θ_R is the contact angle hysteresis, and γ_{LV} is the surface tension of test liquid.

Confocal Microscopy Technique

Confocal laser scanning microscopy (Axiovert 200M, Carl Zeiss, Germany), working in the reflection mode configuration (Inaba et al., 2013), was a tool for the biofilm surface architecture analyses.

The flow cell is also used for continuous microscopic observations of biofilm formation and structure evolution on glass slides under particular shear water flow rates controlled with a peristaltic pump (Yawata et al., 2016). More detailed surface geometric, structural and morphological signatures are evaluated with advanced image analysis programs (COMSTAT, CMEIAS, PHLIP, ImageJ).

In particular, ImageJ allows to create image stacks (z axis) leading to 3D projections of the surface morphology by means of confocal microscopy registrations. The obtained 3D images can reveal details of biofilm matrix geometry, and further used in combination with fluorescence staining visualization, makes the concentration distribution of particular biofilm species like bacteria, algae, or ions to be quantified (Swearingen et al., 2016).

Photoacoustic Spectroscopy System

Photosynthesis generates phenomena which may be detected with a photoacoustic technique. Light energy converted to heat leads to the thermal expansion of tissue, liquids and gases, and is termed the photothermal signal. This is generated when the photosynthetic sample is irradiated by a light pulse. Not all of the light energy absorbed by the sample tissue stored as the process products. The variable unused fraction of the absorbed beam is converted to heat leading to a detectable pressure drop. When a photosynthetic system is illuminated by a pulsed light source, the resulting photosynthetic photolysis of water causes the evolution of a burst of gaseous O_2. The process results in an increase in pressure which is detected by a microphone as a photobaric signal (Pinchasov et al., 2005).

In the photoacoustic spectroscopy (PAS) the thermal diffusion length μ (a certain sample thickness,which affects the signal amplitude at a fixed modulation frequency, can be written: $\mu = (\alpha / \pi f)1/2$ where: $\alpha = k / \rho c$ is the thermal diffusivity ($m^2 s^{-1}$), k is the thermal conductivity (J s^{-1} m^{-1} K^{-1}), c is the specific heat capacity (J kg^{-1} K^{-1}), ρ is the density (kg m^{-3}), f is the frequency of light modulation (varied from 1 to 1kHz). The amplitude of PA signal is proportional to the optical density of the sample (index s) $p_A \sim \mu_S / k_S$ (Szurkowski et al., 2001). By changing the frequency of light modulation, the PA depth profile can provide information on the location of pigments in the biofilm structure (Charland and Leblanc, 1993). The application of different photoacoustic spectroscopy systems for analytical measurements is recently reviewed in (Haisch, 2012).

Interpretation of the data is based on the results originating from a classical Rosencweig-Gersho model (Rosencwaig, 1980). The PAS experimental arrangement constructed for these biofilm studies was described in detail elsewhere (Szurkowski et al., 2000).

The modulated light beam illuminating the biofouled sample placed in a closed-type PA cell leads to the light energy absorption in such a photosynthetic system composed of pigments. There are two parts of the absorbed energy emission, the first one is emitted as the thermal signal (originating from the thermal deactivation of pigments), and the second one spent in photochemical processes (emission of oxygen). Both kinds of emissions and the subsequent acoustic pressure are detected using a microphone. Energy storage (ES) was determined, by measuring heat emission in a closed-type PA cell exposed to modulated and non-modulated background light, as the ratio (A-B)/A * 100(%). A is the PA signal originated from the modulated light switched on together with the non-modulated background light of 2000 μmol photons m^{-2} s^{-1}, whereas B is the PA signal when the cell is illuminated only with the modulated light beam. The modulated light intensity was 25 μmol photons m m^{-2} s^{-1}. The strong background light applied to the sample leads to the saturation state of the photochemical reactions in the sample. Such a strong irradiation increases the conversion effectiveness of the adsorbed light energy to heat to almost 100%. Under the applied condition, the maximal PA is obtained proportional to the modulated light absorption in the probe. All the measurements were performed at room temperature using the measuring light wavelength of 680 nm, for the modulation frequency of 80 Hz i.e., height enough to neglect the oxygen signal contribution, as assumed by others (Veeranjaneyulu et al., 1991). The PA signal amplitude and phase is evaluated by means of the phase-sensitive method realized using a lock-in amplifier. A schematic diagram of the PA system is shown in **Figure 5A** with a laboratory-build closed-type photoacoustic cell, presented in **Figure 5B**.

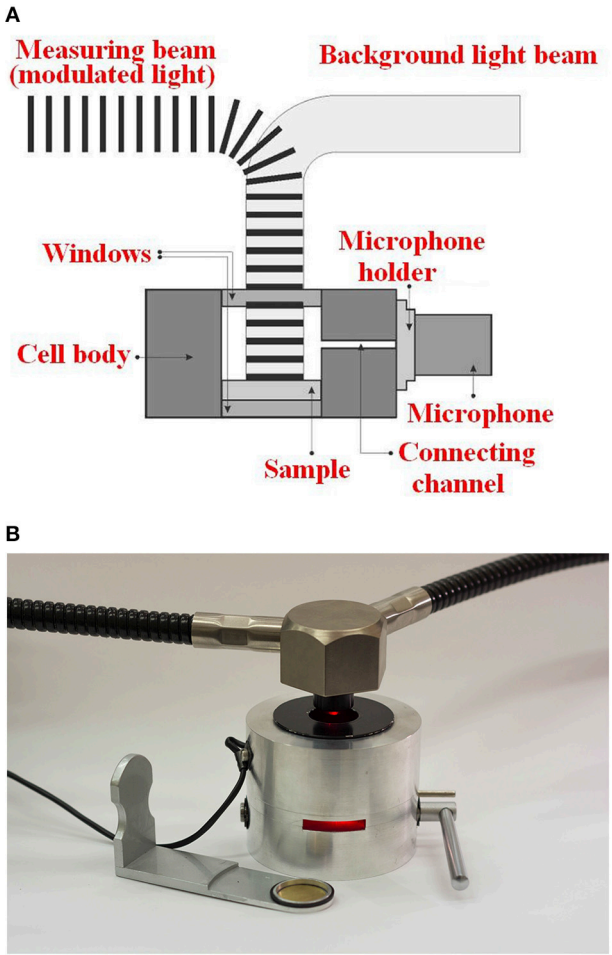

FIGURE 5 | (A) Schematic diagram of PA system. **(B)** Laboratory-built closed-type photoacoustic cell.

As an abiotic substratum for biofilm collection, disks of the same diameter = 18 mm made of glass, aluminum, and brass were chosen. Samples from the seawater planktonic phase were processed following the procedure introduced by Carpentier et al. (1989), where the filtered biological material covered a membrane filter (Sartorius SM 11306). A piece (15 mm ring in diameter) was cut out from the filter, for further PA measurements. Samples made of marine seaweed *Fucus vesiculosus*, *Cladophora sp.*, *Enteromorpha sp.* algae collected at the same location were also studied with the photoacoustic spectroscopy technique, for comparison.

RESULTS AND DISCUSSION

Wettability of Biofouled Surfaces

Since the marine biofouled solid substrata stand for highly heterogeneous, fully-hydrated and porous interfacial systems, the particular CA measuring technique i.e., a captive bubble method turned out to give accurate and reproducible results (Pogorzelski et al., 2013).

CA changes resulting from a variety of fouling conditions are discussed in Thomas and Muirhead (2009). In general, surface fouling can decrease CA when crystalline structures or biofilms are formed. However, at late stages of biofilm formation the outermost surface is enriched in EPS of polymeric and hydrophobic nature. Such a surface coverage has lower γ_{SV} and higher CA, as observed in this study.

In the previous marine biofilm wettability studies), dynamics of the selected parameters variability, for samples registered in the short-time marine biofilm formation interval (to 80 min.), is depicted in Figures 3A–D of Pogorzelski and Szczepanska (2014). The particular biofilm development stages can be identified. At short times, an increase of the both dynamic CAs points to the conditioning film formation step, and after $t = 20$ min. a tendency to attain the constant CA value can be noticed. **Figure 3B** reveals two CAH minima at $t = 5$ and 43 min., which seems to be related to the best-release surface feature. In addition, the time interval between the both stages $\Delta t = 38$ min. could be related to the growth rates ($\sim 1/\Delta t = 2.78 \times 10^{-4}$ s^{-1}) of the microorganisms colony, since the similar values were reported for *Cyanobacteria* (8×10^{-6} s^{-1}) and EPS (12×10^{-6} s^{-1}) in Wanner et al. (2006). Gao and McCarthy (2006) argued that CAH is closely related to the bioadhesion of OM to the solid substratum. It was evidenced that CAH less than 10°Could lead to removal of biofilm covering submerged macrophyte leaf blades by shear water flow (Genzer and Efimenko, 2006). Schmidt et al. (2004) found that the bioadhesive properties the surface are correlated to CAH rather than to the surface energies of the coatings. The outermost surface appeared to be most hydrophobic (minimal γ_{SV}) at $t = 43$ min., as shown in Figure 3C, which is correlated with the maximum at Π (t) plot from Figure 3D i.e., the mature biofilm stage, where the surface bioaccumulation ($\sim\Pi$) attains the saturation value. Finlay et al. (2002) addressed the solid surface energy effect on biofilm accumulation using a variety of model materials of differentiated hydrophobicity. As a result, the hydrophobic surfaces tend to accumulate polymeric-like compounds whereas the hydrophilic ones are enriched in polar biomaterials (Krishnan et al., 2008). The lowest bioadhesion is foreseen for solid substrata with γ_{SV} from the range [20–30 mJ m^{-2}; Baier (1970)]. The model substrata used here had surface energy values: 58.8 (wood), 55.9 (glass), 43.3 (aluminum), 41.8 (brass), and 38.6 (stainless steel) mJ m^{-2}, and demonstrated significant bioaccumulation. 2D adsorptive film pressure Π, according to the Gibbs adsorption theory (Adamson and Gast, 1997), is related to the surface adsorption Γ (Gibbs excess) $\sim\Pi/RT$, where: R is the gas constant and T is the absolute temperature. Our comprehensive biofilm studies confirmed that the biofilm wet weight (BWW) was positively correlated to Π. An increase of surface roughness (derived from confocal microscopic studies) resulted in CAH ↑. Bioaccumulation progressing in time of biofilm formation (expressed by BWW) pointed to the hydrophobization (γ_{SV} ↓) of the outermost biofilm surface likely enriched in EPS compounds. It should be pointed out that several other factors which could affect the biofilm formation process and final composite structure like surface energy, electricity, shear flow velocity, roughness etc., as can

be learned in Zhao et al. (2005) and Thomas and Muirhead (2009).

A general trend in the wettability parameters variability can be noticed: $\Theta_A \uparrow$, $\Theta_R \uparrow$, CAH $\uparrow$, $\Pi \uparrow$ $\gamma_{SV} \downarrow$, $W_A \downarrow$, and W_S become more negative with an increase of the biofilm age at longer time-scale periods (days).

The biofilm treatment procedure has a significant influence on CA, vacuum drying of fouled surfaces increases CA by about 8° (Donlan, 2002). Surface roughness is another important factor influencing CA, especially on a complex surface of biofilms. In tests, where defect heights was used in ratio to capillary length, larger defect heights served to increase CA, likely creating pinning edges (Cubaud et al., 2001). In Thomas and Muirhead (2009), the empirical equation for CA was developed with two parameters characterizing the biofouled surface i.e., the area fraction fouled f_{fouled}, and d/l_{cap}-the ratio of defect height to capillary length, which supports the observation that wastewater fouling can generally decrease CA from the baseline on a clean but corrugate surface. Biofouling studies of six different abiotic substrata with varying surface energy (18–40 mJ m^{-2}) and surface roughness (45–175 μm) were performed in coastal sea waters (Lakshmi et al., 2012). The correlation analyses performed on biofilm parameters (carbo hydrate, total viable bacterial count, organic matter etc.) exhibited that surface energy and CA are highly correlated, viable count of bacteria was positively correlated to surface energy ($R = 0.69$). The attachment of macrofouler and the surface characteristics are also well correlated with surface energy and roughness.

A large variety of organisms can compose the marine biofilm colony of different size and shape like: bacteria (1 μm), yeast (3–5 μm), fungi (12–18 μm), algae (∼25 μm), cilitae (>200 μm) living apart from macroorganisms (barancles or seaweeds) that is important in the light of surface roughness of substrata to be inhabited (Wanner et al., 2006).

Data on the marine organisms classes and their occurrence in different seasons at the south Baltic region can be found in Kautsky and Kautsky (2000). In the study area, monocell algae were present composing microphytobenthos. *Diatomophyceae* and *Dinophyceae* dominated phytoplankton of the Baltic with a significant account of *Cyanobacteria*. Seasonality of organisms taxes can be noticed: diatoms are found in spring, *Cyanophyta* in summer, and diatoms prevail in autumn.

Spearman's rank correlation coefficients (R) between the trophic status indicators and the surface wettability parameters of the glass substrata submerged in Baltic Sea coastal waters are listed in **Table 1**. All the parameters are negatively correlated to Secchi depth, although the absolute values indicated a strong correlation effect only for the wettability parameters: CAH, γ_{SV}, Π (with R = 0.68–0.96). The remaining ones i.e., W_A are W_S are much less correlated to the trophic status indicators ($R =$ 0.40–0.69). Moreover, the wettability parameters are correlated to each other (data not shown here). That concerns Θ_A, Θ_R, CAH, and W_A. It may be concluded that a set of the surface wettability parameters can be limited only to the uncorrelated quantities since the other ones born no more information on the solid surface/water phase interactions. A larger comprehensive data set is required to establish the functional relations between the trophic status parameters and the surface wettability energetic ones of practical value.

TABLE 1 | Spearman's rank correlation coefficients between the trophic status indicators and wettability parameters of glass substrata submerged in Baltic Sea coastal waters.

Trophic State Indicators	CAH (deg)	Π (mNm^{-1})	γ_{SV} ($mJ\ m^{-2}$)	W_A ($mJ\ m^{-2}$)	W_S ($mJ\ m^{-2}$)
1. pH	0.631	0.673	0.712	0.551	0.684
2. Dissolved O_2 (mg dm^{-3})	0.845	0.781	0.893	0.613	0.697[b]
3. Secchi depth (m)	−0.621	−0.755	−0.825	−0.654	−0.715
4. Total P (mg dm^{-3})	0.751	0.912[a]	0.789	0.572	0.542[b]
5. Total N (mg dm^{-3})	0.824	0.933[a]	0.726	0.683	0.402[b]

[a]$p < 0.05$, $n = 9$; [b]$p < 0.01$, $n = 6$.

So far, the wetting properties of solid substrata (minerals) found in marine waters affected by natural surfactant adsorption were determined under laboratory using the dynamic CA approach (Mazurek et al., 2009). Recently, the condition level of submerged in sea water surfaces were evaluated via the surface wettability parameters (Pogorzelski et al., 2013). Moreover, the novel contact angle hysteresis methodology based on wettability energetics allowed us to quantify the atmospheric environment pollution impacts on *Pinus Silvestris L.* needles (Pogorzelski et al., 2014), and seems to be a technique of general concern applicable to a large variety of complex interfacial systems.

Confocal Microscopy Biofilm Characterization

The non-invasive visualization of biofilm development by applying the technique of continuous-optimizing confocal refection microscopy (COCRM) was used to derive the input biofilm features essential in mathematical modeling of biofilm formation kinetics (Inaba et al., 2013).

Confocal microscopy sections (along z-axis with a 3 μm separation) through a marine biofilm on glass (14 – day formation time) from top (1) to bottom (11) are shown in **Figure 6A**; HF represents a split of an image stock from (1) to (11) derived with Helicon Focus program covering area 425 × 570 μm. 3D reconstructed surface morphology exhibiting an exopolymer matrix with water cannels was obtained by ImageJ program (**Figure 6B**). Much more detailed information on the particular biofilm architecture can be obtained using several image processing programs applied to 3D stacks of biofilm images, as demonstrated in Heydorn et al. (2000), Mueller et al. (2006); Lamprecht et al. (2007) and Dazzo (2010). For instance, the use of PHLIP permitted the dynamics and spatial separation of diatoms, bacteria, and organic and inorganic components to be followed (Mueller et al., 2006).

The geometric-morphological biofilm parameters, for the particular structure in **Figure 6**, are as follows: mean thickness = 14.2 μm, biovolume = 46,700 μm^3, coverage area fraction f =

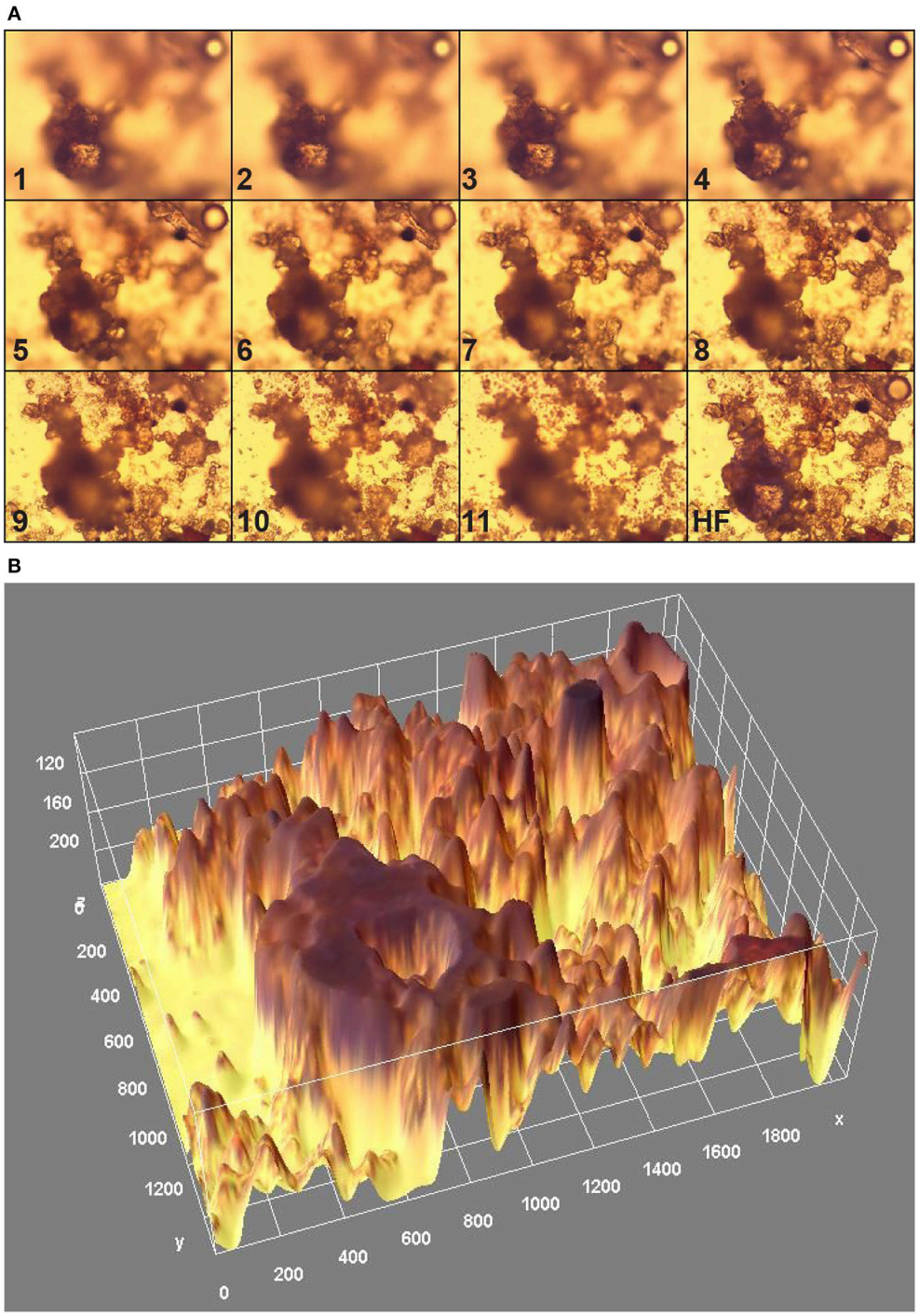

FIGURE 6 | Optical confocal microscopy sections through a marine biofilm on glass: **(A)** stock of sections from (1) to (11) spitted to (HR) with Helicon Focus routine; z-axis separation = 3 μm, **(B)** 3D reconstructed surface architecture with ImageJ program from HF covering area = 425 × 570 μm (Magnification = 400 times; x, y, and z axes in pixels i.e., 180 pixels = 50 μm).

60.2 %, roughness parameter r = 0.49, fractal dimension = 1.36, Hopkins aggregation index = 2.89.

The fractal dimension (varying between 1 and 2) reflects a contact line complexity of the object with the surrounding area, higher values point to a more developed border line (Yang et al., 2000). Hopkins' index is a measure of biofilm colony dispersion state, for randomly distributed structures is <2 (Dazzo, 2010).

Generally, the algal community evaluated to larger species which correlated to an increase in biovolume ($R = 0.96$), and demonstrated the biofilm thickness grow ($R = 0.87$) with time. Bacteria were appeared at measurable quantities close to the solid surface, whereas microalgae occupied intermediate parts of the layered structure. EPS covered the outermost surface of the microcolony exposed to the surrounding water. The principal biofilm compounds demonstrated differentiated kinetics with the time elapsed. A clear transition was observed from a heterotrophic community (enriched in bacteria) to an autotrophic community consisting largely of diatoms. The biofilm development leads to an increase in its heterogeneity since a strong correlation between roughness and biovolume was noticed.

Not all the structural-geometric biofilm parameters are useful as the novel water body trophic status indicators. These comprehensive studies demonstrated that a strong positive correlation appeared between: biovolume vs. biofilm wet mass (BWW) ($R = 0.78$), coverage fraction f vs. BWW ($R = 0.82$), biofilm thickness vs. Π ($R = 0.86$), and biofilm thickness vs. γ_{SV} ($R = -0.83$).

An attempt was made to map the surface spatial heterogeneity with both the captive bubble wettability sensor, and confocal microscopy system on the same biofilm-covered glass sample. The biofilm thickness along the straight line marked on the glass slide surface (**Figure 7A**) correlates well with the surface pressure Π (x-axis) profile (compare **Figures 7B**,**C**); although the thickness is apparently negatively related to the surface energy of the sample (**Figure 7D**).

Modeling of Biofilm Formation Dynamics

There are two commonly-used biofilm modeling techniques based on a dynamic systems formalism where the concentrations variability of the species are expressed with different relations and a so-called individual—based approach which appears to be of particular value in describing multicomponent systems undergoing several structural transitions of differentiated time-scales (Garrett et al., 2008; Lodhi, 2010).

The model analyzed in this report is based on the general principle of mass conservation for soluble and particulate biofilm components (Wanner et al., 2006).

The biofilm formation process in a seawater environment is a complex phenomenon, where several species are involved like: bacteria, fungi, diatoms, protozoans, larvae, and algal spores (Railkin, 2004). In addition, the process is mediated by physicochemistry of a substratum along with the environmental conditions such as a nutrient level, pH, dissolved O_2, light availability, sample depth, and temperature (Chiu et al., 2005).

From the previous work (Pogorzelski and Szczepanska, 2014), the CA wettability sensor appeared to be effective in *in-situ* and continuously biofilm formation studies and was used here simultaneously with a fluorescence-based microscopy technique. The experimental methodology and data evaluation procedure was adapted after (Fischer et al., 2014) to identify the known phases of biofilm development and to determine the specific growth rates μ, and the conditioning or induction times λ, where Gomperts sigmoidal function was selected to describe a specimen growth curve (Zwietering et al., 1990). The specific growth rate starts at a value of zero and then accelerates to a maximum value μ_m in a certain period of time, resulting in a lag time (λ). Values of μ_m and λ were recovered from the growth dynamics curve G(t), as presented in Fischer et al. (2014). The colony organism growth curves can show a decline that leads to different μ and λ values.

The experimental observations in these studies revealed that in natural multispecies ecosystems, the surface colonization kinetics ought to be approximated with at least three Gompertz functions that remained in agreement with previous findings of Fischer et al. (2014). A split of G(t) functions is required to display the main steps of microcolony formation (Fischer et al., 2014):

$$G(t) = \sum_{i=1}^{3} g_i(t) \text{ where} \tag{1}$$

$$g_i(t) = (A_i - A_{i-1}) \exp\left\{-\exp\left[\frac{\mu_i \cdot e}{A_i - A_{i-1}}(\lambda_i - t) + 1\right]\right\}$$

Here, $g_i(t)$ is a logarithmic function of the biofilm signal (film-covered area fraction f) corresponding to the sigmoidal growth taking place in the *i*th stage of biofilm development. The remaining parameters are defined in Fischer et al. (2014).

The biofilm structure development dynamics was followed simultaneously with three sensors (confocal microscopy, wettability CA technique, and photoacoustic spectroscopy) to validate the model and determine the biologically significant parameters. For instance, EPS deposition pattern in a biofilm can be quantifiable by application of potassium permanganate, $KMnO_4$, yielding brown MnO_2 precipitate deposition on the EPS, which was evaluated using data from a reflection detector (Swearingen et al., 2016). On the basis of an increase in the red band PA spectra from chlorophyll-containing cells, the growth in a cell size was determined.

An exemplary marine biofilm growth curve is shown in **Figure 8**. From the plot, biological parameters μ_i and λ_i were derived, as shown in Figure 1 of Zwietering et al. (1990), for the main stages of the biofilm establishment and identified specimens. They are collected in **Table 2**, and remain in agreement with the published data by others on the time-scale of transition processes in biofilms (Wanner et al., 2006; Klapper and Dockey, 2010).

At least, seven main phases of marine biofilm structure can be defined (Fischer et al., 2014), and four identified in our studies are visualized in **Figure 8** as insets. Starting from the biochemical conditioning (phase I), subsequently a pioneer attachment phase appears (phase II) followed by the adaptation phase (phase III). The exponential-like accumulation growth stage (phase IV) leads to the asymptotic maximal bacterial cell density (in phase V). In this phase, the surface is to a great extend colonized by unicellular diatoms. The presence of phase VI is attributed to the accumulation of eukaryotic microorganisms, and finally phase VII representing the exponential accumulation stage of, which stand for the pseudo-stationary stage of mature biofilm structure. The latter phases are mediated by environment-specific

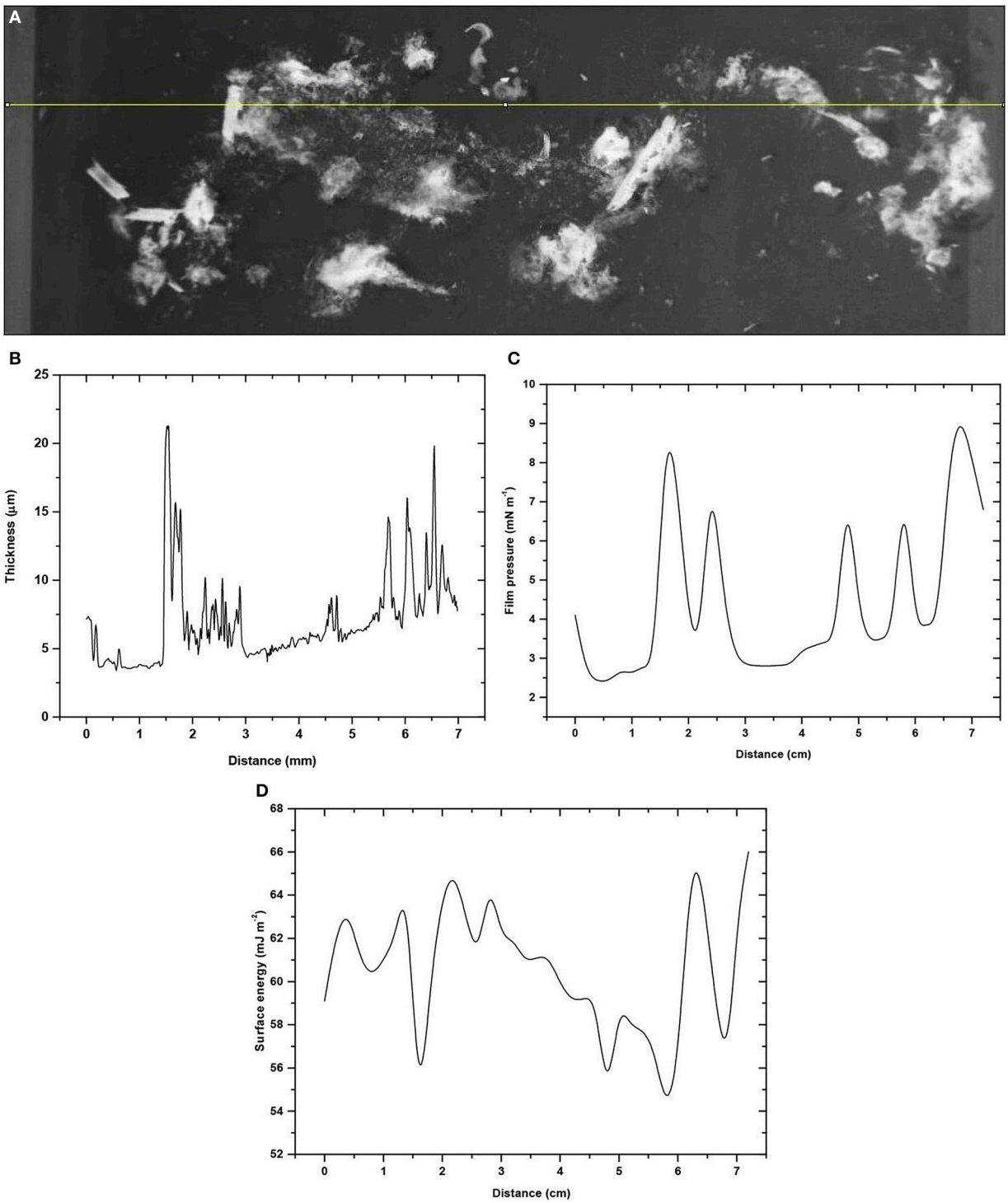

FIGURE 7 | Spatial mapping of marine biofilm heterogeneity on glass. **(A)** Optical profile along a horizontal line. **(B)** Biofilm thickness profile from confocal microscopy. **(C)** Surface pressure and **(D)** Surface energy profiles both derived with the wettability captive bubble sensor.

factors like seasonal, local and biological activity in seawater and plankton availability. It should be born in mind that not all the phase may necessarily occur in particular marine ecosystems. Biofilm formation dynamics studies performed in a low primary production season (November-December) demonstrated no settlements of larger microorganisms. The similarity of biofilms on different substrata in seawater was observed for early stages of a colony formation (up to 4 d), where a conditioning film of organic matter is quickly generated. This film masks the surface chemistry of the substratum (Jones et al., 2007). As a result,

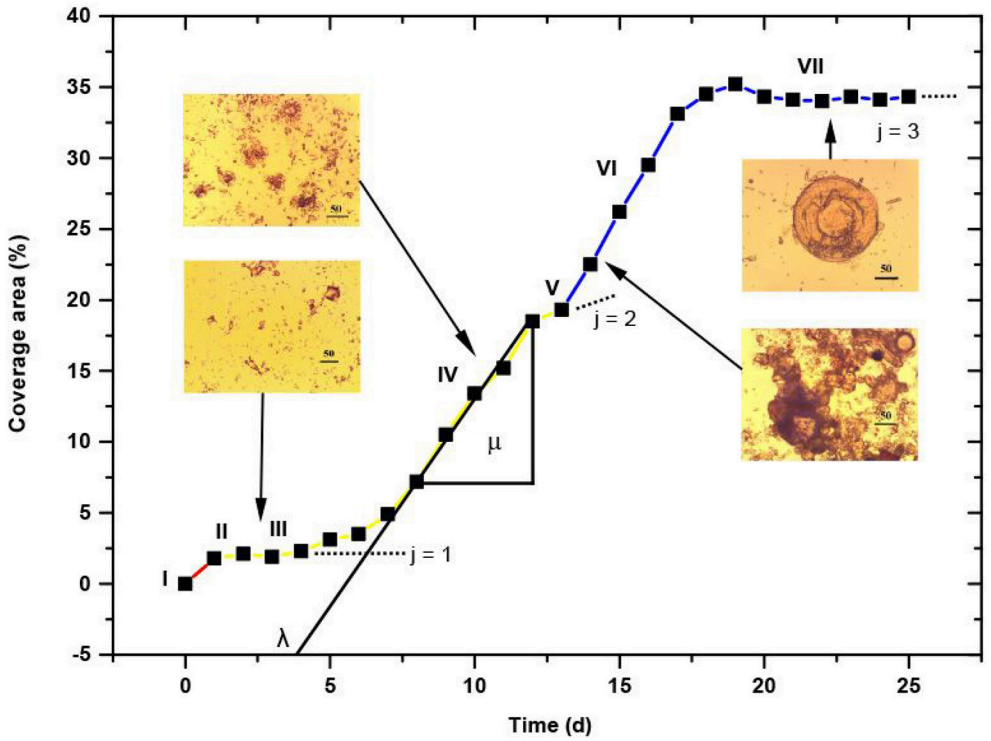

FIGURE 8 | Marine biofilm growth curve (coverage area fraction vs. time) fitted with three Gompertz functions. Red, orange and blue line parts correspond to the main stages of biofilm establishment. I-VII seven main phases of biofilm formation dynamics. Microscopic images of four characteristic stages of the growth phases (Magnification 400 x, bars correspond to 50 μm) are shown as insets.

TABLE 2 | Characteristic time-dependent features of marine biofilm formation.

No	Biofilm process time scale	Sensor
1	Biochemical preconditioning to 5 min. $\mu = 0.27 \pm 0.09\ h^{-1}$	Contact Angle
2	Initial bacteria colonization 5 to 40 min.	Contact Angle, Confocal Microscopy
3	Bacteria colonization cycle 1 h	Contact Angle
4	Cyanobacteria growth 34.5 h	PA Spectroscopy
5	EPS growth 23 h; $\lambda_1 = 2.8 \pm 0.2$ d, $\mu_1 = 0.56 \pm 0.12\ d^{-1}$ $\lambda_2 = 6.4 \pm 0.4$ d, $\mu_2 = 0.27 \pm 0.82\ d^{-1}$	Confocal Microscopy Contact Angle
6	EPS death 11.5 d	Confocal Microscopy, Contact Angle
7	Diatom growth 57 d	PA Spectroscopy, Confocal Microscopy
8	Diatom consumption 12.5 d	PA Spectroscopy

colonizing bacteria could perceive them as similar, and other factors as electricity, roughness, color etc. could mediate further colonization.

Chlorophyll a is most commonly used to estimation of algal biomass, thus the *Chlorophyll* content may be inversely proportional to light intensity. Chemical composition of biofilms can be used as an indicator of nutrient uptake efficiency. Largely, elemental ratios of nutrients such as carbon and nitrogen (C/N), and nitrogen and phosphorus (N/P) are calculated (Burns and Ryder, 2001).

Biofilm as a Photosynthetic System

Energy Storage ES of Biofilms

Photoacoustic PA technique turned out to be an effective tool in photosynthetic systems investigations particularly to direct determination of ES (Carpentier et al., 1989; Veeranjaneyulu et al., 1991), and oxygen emission in untouched leaves (Poulet et al., 1983; Mauzerall, 1990).

The energy storage of the sample indicated a linear dependence on the photosynthetic system capacity taken at the maximum rate corresponding to stable photochemical products generation (Szurkowski and Tukaj, 1995).

The exemplary energy storage (ES) determination plot is shown in **Figure 9**, for a biofilm sample stored in Baltic Sea coastal waters for 14 days (studied on August 25, 2015).

Short-time ES evolution studies showed the fast ES increase up to 3–4 h then reaching an almost constant value in the middle of the biofilm cycle. ES measurements were carried out for the sample in its steady state. ES data were evaluated at different seasons, for biofilms collected at solid substrata (glass, macrophyte leaves), and organic matter filtered from a planktonic phase met at adjacent waters, for comparison, are summarized in **Table 3**.

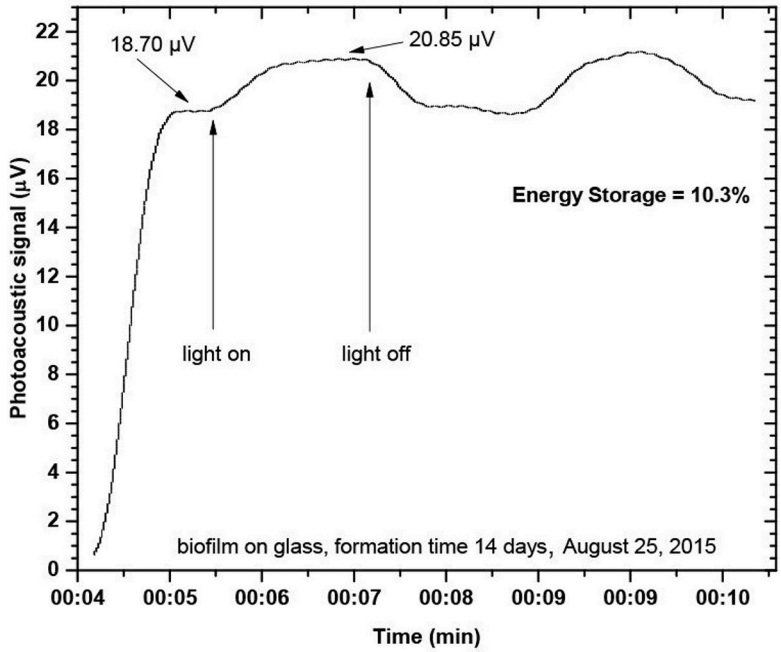

FIGURE 9 | Photoacoustic ES plot, for marine biofilm collected at a glass substratum (Baltic Sea, Gulf of Gdansk, sample age- 14 days).

TABLE 3 | ES of marine photosynthetic systems studied in Baltic Sea coastal waters registered along a time period from spring to autumn seasons.

No.	Species	Energy storage (%)
1	Biofilm on glass (14-d formation; Baltic Sea; 27 July 2015)	18.4 ± 4.6
2	Planktonic phase (50 cm^3 volume deposition on membrane filter; 27 July 2016; Baltic Sea)	15.1 ± 2.8
	Planktonic phase (150 cm^3 volume deposition on membrane filter; 25 August 2016; Baltic Sea)	10.3 ± 1.9
	Planktonic phase (150 cm^3 volume deposition on membrane filter; 23 September 2016; Baltic Sea)	10.4 ± 1.6
	Planktonic phase (250 cm^3 volume deposition on membrane filter; 21 October 2016; Baltic Sea)	6.2 ± 1.1
3	Biofilm on glass (14-d formation; August, 2015)	19.6 ± 5.0
4	Biofilm on glass (14-d formation; September, 2015)	21.3 ± 5.6
5	Biofilm on glass (14-d formation; October, 2015)	20.5 ± 4.6
6	Biofilm on glass (14-d formation; November, 2015)	12.2 ± 4.8
Macroalgae		
7	*Cladophora sp.* (July, 2015)	23.1 ± 4.0
8	*Fucus vesiculosus* (July, 2015)	21.8 ± 5.2
9	*Zostera marina* (July, 2015)	11.3 ± 3.5

Generally, ES values were higher, for a season of high primary production. The maximum was attained in September, for biofilm on glass samples, although for the planktonic phase matter it was observed in late July. In addition, ES values were found higher by a factor of 1.5–2, for the biofilm settled on solid substrata, in particular on biotic macroalgae blades, for probes taken at the same place, time, and environmental conditions. The obtained ES values lie in the range reported by Cullen (1990). Comprehensive algal (*Macrocystis pyrifera* and *Ulva sp.*) studies revealed similar ES variability (Herbert et al., 1990). Seasonal O_2 and ES evolution during the cell cycle of green alga *Scendesmus aramtus* was already characterized by photoacoustic spectroscopy (Szurkowski et al., 2001). ES could be an indicator of water pollution, as demonstrated by Szurkowski and Tukaj (1995), for plants exposed to contamination. They are lower than or equal to those measured for samples in a pollution-free environment. The best correlation between ES and pollution levels was obtained for a batch culture of green microalgae *Scenedesmus armatus* (Szurkowski and Tukaj, 1995).

It can be noted that photosynthetic energy storage efficiency mediates the development of phytoplankton cultures. All the abiotic environmental factors like: temperature, nutrient availability and contamination level will be reflected in detectable changes in photosynthetic energy storage efficiency of phytoplankton, and further affects the total biomass and composition of biofilm cultures (Pinchasov et al., 2007). The effect of nutrient limitation on relative photosynthetic efficiency was exhibited as a significant drop in ES (by 50%) in P- limited, and (by 60%) in N-limited algal cultures, as compared to the reference one (Pinchasov et al., 2005). In the photoacoustic method, ES efficiency is independent of chlorophyll concentration, and the observed ES decrease did not result from death of some cells within the population but due to inactivation of increasing fractions of the photosynthetic units.

PA Spectral Characteristics of Biofilms

Bioptical properties of a microorganism colony at solid substrata were already studied with acoustic spectroscopy methods (Schmid, 2006; Bageshwar et al., 2010) apart from the conventional optical ones (Ionescu et al., 2012). The photo thermal signal amplitude can be a good measure of the culture biomass, dimensions of the cells and oxygen evolution therein (Szurkowski et al., 2001). Periphyton is a complex mixture of algae, cyanobacteria, heterotrophic microbes, and detritus containing a mixture of pigments (see in **Figure 10**, where the combined absorption spectra of natural pigments, modified after (Schagerl and Donabaum, 2003; Schagerl et al., 2003) are shown.

The high correlation between the photosynthetically active biomass, expressed in *Chlorophyll a* content, and the absorption coefficient at the corresponding absorption wavelength of *Chl a* (673 nm) already made possible the estimation of biomass from reflectance measurements (Kazemipour et al., 2011).

Exemplary marine biofilm on glass PA amplitude (blue) and phase (red) spectra obtained in summer **(A)** and autumn **(B)** seasons are shown in **Figure 11**. In determining a photoacoustic spectrum, the original photoacoustic signal has to be divided by the spectrum of the excitation light beam (routinely by the spectrum of the reference sample i.e., carbon black) in order to eliminate a discrepancy attributed to differential light intensity throughout the source spectrum (Rosencwaig, 1980), so the PA amplitude is in (a.u.). The spectrum exhibits three maxima at wavelengths ca 430, 490, and 690 nm. The first and third of these maxima corresponds to absorption by *Chlorophyll a*, that at

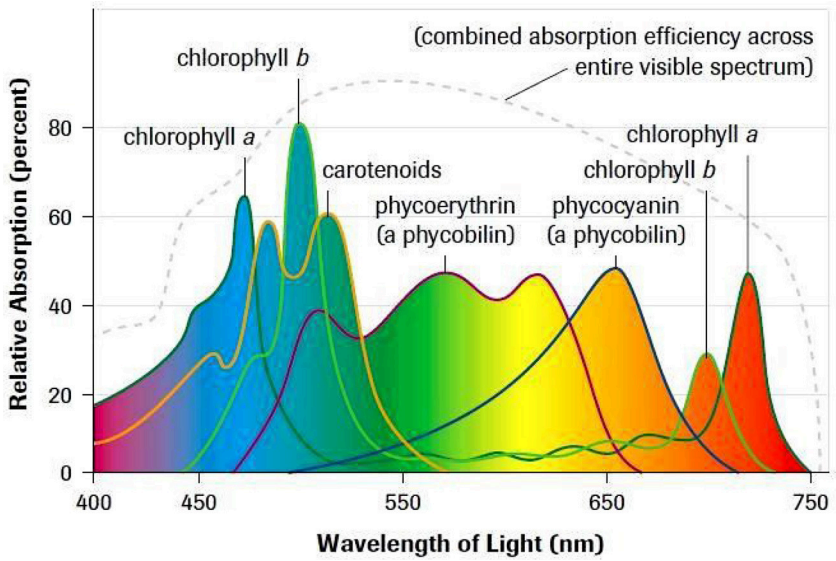

FIGURE 10 | Natural pigments absorption spectra, where the accessory pigments are combined with *Chlorophylls a and b*; modified after (Schagerl et al., 2003).

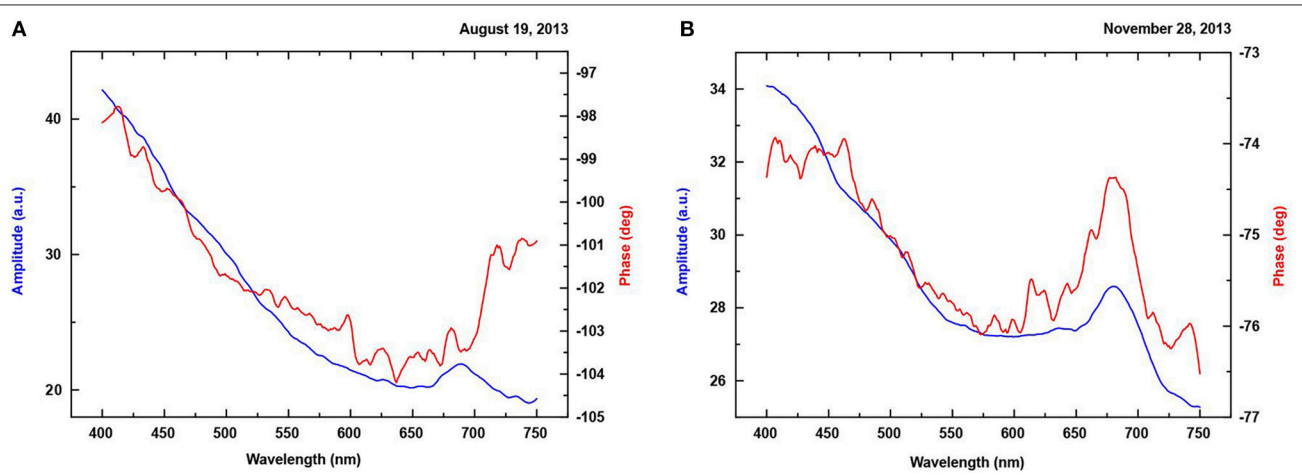

FIGURE 11 | Marine biofilm PA amplitude and phase spectra registered at the same station (Orlowo, Gulf of Gdansk, biofilm age-−14 days, collected on glass) in different seasons: **(A)** summer and **(B)** autumn.

480–490 nm to absorption of pigments accessory to *Chlorophyll a*.

Significant differences between PA amplitude spectra can be noticed. The lower maximum, for *Chlorophyll a* at 675 nm, for the sample collected on 19 Sept. 2013 in reference to the one on 28 Nov., 2013 can result from: 1. a lower *Chl. a* content in this time or 2. Very effective process of oxygen production (Szurkowski et al., 2001). A seasonal succession of phytoplankton groups in the studied water body (Fischer et al., 2014), reveals the presence of cyanobacteria, dinoflagellates, and bacillariophyceae in September but diatoms are found only in November. It should be noticed that the PA amplitude is dependent on the photoacoustically-induced heat production (proportional also to biomass) but the PA signal phase is proportional to oxygen production effectiveness (Poulet et al., 1983). The phase of the PA signal is more sensitive to the changes of optical and thermal properties of the layered sample than the magnitude of the PA signal (Du et al., 1995). The absolute value of the PA signal phase increment is caused by the additional signal due to the oxygen evolution. It means that the lower PA amplitude maximum in September does not result from the lower algae content in the biofilm but from the fact that a significant part of the heat energy was spent on the photosynthesis process (oxygen production). This statement was confirmed by the PA signal phase spectra. The maximal phase change, observed in September, was about 6° (from -104° to -98°) but in November only 3° (from -77° to -74°). It points to the higher oxygen production in the photosynthetic biofilm system taking place in September.

Since cyanobacteria are incorporated into the biofilm structure together with green bacteria containing *Chlorophyll a* (Ionescu et al., 2012), the biofilm pigment composition can be derived from the spectral maxima ratio: (*Bacteriochlorphyll c*/*Chlorophyll a*), (Kazemipour et al., 2011).

Effectiveness of the photosynthetic part of biomass accumulation in a biofilm structure is a substratum-specific quantity, as demonstrated in **Figure 12**. The peak values in the PA signal amplitude spectra maximum at ∼680 nm were found highest for a biotic substratum (wood), lower for the filtered planktonic phase, and lowest for the metallic abiotic surfaces. A close positive correlation was found between the said spectral peak value and BWW (R= 0.89). Such a relation is helpful in the best efficient collecting sampler material selection (depending on surface free energy, roughness, surface electricity etc.), for a particular water body (sea, inland waters).

The photoacoustic parameters (ES and PA signal amplitude spectra maxima, in particular) turned out to be unequivocally related to the biofilm structural signatures (free energy of the outermost biofilm surface, biofilm wet weight, fractional biofilm area coverage). In conclusion, the photoacoustic method proves to be a source of valuable information on the photosynthetic apparatus of biofilm colony (as ES, diffusion parameters, photochemical loss) during its life cycle not accessible by other methods.

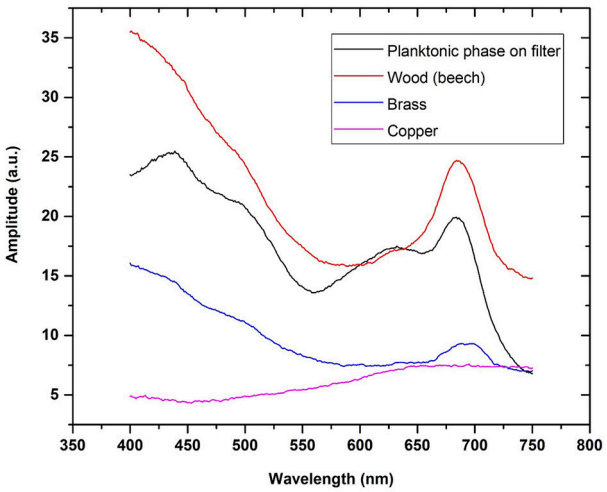

FIGURE 12 | Biofilm substratum effect on PA signal amplitude spectra. Biofilm samplers deployed in Baltic Sea coastal waters; sampling time 14 days.

CONCLUSIONS

The CA wettability sensor is capable of quasi-continuous biofilm evolution monitoring from the conditioning film stage to fully-developed 3D structured multispecies clusters. *In-situ* and *on-line* measurements can be performed on permanently submerged solid substrata, so-called biointerfaces (epilithon, epixylon, epipsammon, and epiphylon).

Confocal reflection microscopy assisted with imaging picture processing allowed us to indentify known phases of a biofilm development and to determine parameters of biological meaning (specific growth rates, induction time) applying a superposition of Gompertz functions to mathematical modeling of biofilm growth dynamics.

3D biofilm architecture can be quantified with several structural-geometric parameters (biovolume, roughness, thickness, substratum coverage, fractal dimension, Hopkins aggregation index etc.) which turned out to be unequivocally related to physicochemical surface properties of the substratum and environmental conditions, finally correlated to the trophic state indicators of the sea water body.

PA spectroscopy spectra and ES values of the biofilm photosynthetic system exhibited seasonal changes related to OM accumulation, and the transition of biofilm colony community from autotrophic to heterotrophic organisms. It can be expected that the level of main nutrients attributed to biofilm growth (nitrogen and phosphorus), are the principal factors mediating its biomass and ES efficiency. Variability of ES within hours to days is accompanied by changes in biomass or taxonomic composition.

Nutrient limitation and anthropogenic eutrophication are among others the most important factors determining the overall status of water bodies which can be followed by ES efficiency of biofilm cultures.

Cross-correlations found between the chemical water body trophic state indicators and the structural-geometric-wettability-photoacoustic biofilm parameters derived from physical sensing techniques made a promising starting point to propose modern indicators useful in marine waters bioassessment. However, the functional dependences remain to be established, on the larger data base, to apply the results in real ocean science and engineering.

AUTHOR CONTRIBUTIONS

MG prepared the experimental set-up, performed photoacoustic spectroscopy and confocal microscopy measurements and data evaluations. SP formulated work concept, created theoretical background, analyzed and discussed results. AP performed seawater chemical analyses and trophic state evaluations. KB-S performed correlation analyses, searched for literature background interpretation, wrote manuscript. The manuscript has been read and approved by all the listed authors, and the order of authors in the article was also approved.

FUNDING

This work was financially supported by the University of Gdańsk (contract number: DS 530-5200-D464-17).

REFERENCES

Adamson, A. W., and Gast, A. P. (1997). *Physical Chemistry of Surfaces.* 6th Edn Newyork, NY: Wiley and Sons

Azeredo, J., Azevedo, N. F., Braindet, R., Cerca, N., Coenye, T., Costa, A. R., et al. (2017). Critical review on biofilm methods. *Crit. Rev. Microbiol.* 43, 313–351. doi: 10.1080/1040841X.2016.1208146

Bageshwar, D. V., Pawar, A. S., Khanvilkar, V. V., and Kadam, V. J. (2010). Photoacoustic spectroscopy and its applications – a tutorial review. *Eurasian J. Anal. Chem.* 5, 187–203.

Baier, R. E. (1970). "Surface properties influencing biological adhesion," in *Adhesion in Biological Systems,* ed R. S. Many (New York, NY: Academic Press Inc), 15–48.

Burns, A., and Ryder, D. S. (2001). Potential for biofilms as biological indicators in Australian riverine systems. *Ecol. Manage. Restor.* 2, 53–63. doi: 10.1046/j.1442-8903.2001.00069.x

Carlson, R. E. (1977). A tropic state index for lakes. *Limnol. Oceanogr.* 22, 361–639. doi: 10.4319/lo.1977.22.2.0361

Carpentier, R., Leblanc, R. M., and Mimeault, M. (1989). Photoacoustic detection of photosynthetic energy storage in photosystem II submembrane fractions. *Biochim. Biophys. Acta* 808, 293–299. doi: 10.1016/0005-2728(85)90012-X

Charland, M., and Leblanc, R. M. (1993). Photoacoustic spectroscopy applied to biological systems. *Bull. Inst. Chem. Res. Kyoto Univ.* 71, 226–244.

Chibowski, E. (2003). Surface free energy of a solid from contact angle hysteresis. *Adv. Colloid Interf. Sci.* 103, 149–172. doi: 10.1016/S0001-8686(02)00093-3

Chibowski, E. (2007). On some relations between advancing, receding and Young's contact angles. *Adv. Colloid Interf. Sci.* 133, 51–59. doi: 10.1016/j.cis.2007.03.002

Chiu, J. M. Y., Thiyagarajan, V., Tsoi, M. M. Y., and Qian, P. Y. (2005). Qualitative and quantitative changes in marine biofilms as a function of temperature and salinity in summer and winter. *Biofilms* 2, 183–195. doi: 10.1017/S147905050500195X

Cubaud, T., Fermigier, M., and Jenffer, P. (2001). Spreading of large drops on patterned surfaces. *Oil Gas Sci. Technol.* 56, 23–31. doi: 10.2516/ogst:2001003

Cullen, J. J. (1990). On models of growth and photosynthesis in phytoplankton. *Deep-Sea Res.* 37, 667–683. doi: 10.1016/0198-0149(90)90097-F

Dang, H., and Lovell, C. R. (2016). Microbial surface colonization and biofilm development in marine environments. *Microbiol. Mol. Biol. Rev.* 80, 91–138. doi: 10.1128/MMBR.00037-15

Dazzo, F. B. (2010). "CMEIAS Digital microscopy and quantitative image analysis of microorganisms," in *Microscopy: Science, Technology, Applications and Education*, eds A. Mendez-Vilaz and J. Diaz (Badajoz: Formatex Research Center), 1083–1090.

Donlan, R. M. (2002). Biofilms: microbial life on surfaces. *Emerg. Infect. Dis.* 8, 881–890. doi: 10.3201/eid0809.020063

Du, H., Fang, W., and Zheng, J. J. (1995). Photoacoustic phase spectrum of a layered sample. *Appl. Phys. A* 60, 419–423. doi: 10.1007/BF01538344

Finlay, J. A., Callow, M. E., Ista, L. K., Lopez, G. P., and Callow, J. A. (2002). The influence of surface wettability on the adhesion strength of settled spores of the green alga *Enteromorpha* and the diatom *Amphora*. *Integr. Comp. Biol.* 42, 1116–1122. doi: 10.1093/icb/42.6.1116

Fischer, M., Friedrichs, G., and Lachnit, T. (2014). Fluorescent-based quasicontinuous and in situ monitoring of biofilm formation dynamics in natural marine environments. *Appl. Environ. Microbiol.* 80, 3721–3728. doi: 10.1128/AEM.00298-14

Flemming, H. C. (2009). "Why microorganisms live in biofilms and the problem of biofouling," in *Marine and Industrial Biofouling,* eds H. C. Fleming, R. Venkatesan, and K. E. Cooksey (Berlin; Heidelberg: Springer), 3–12.

Gao, L., and McCarthy, T. J. (2006). Contact angle hysteresis explained. *Langmuir* 22, 6234–6237. doi: 10.1021/la060254j

Garrett, T. R., Bhakoo, M., and Zhang, Z. (2008). Bacterial adhesion and biofilms on surfaces. *Prog. Nat. Sci.* 18, 1049–1056. doi: 10.1016/j.pnsc.2008.04.001

Genzer, J., and Efimenko, K. (2006). Recent developments in superhydrophobic surfaces and their relevance to marine fouling: a review. *Biofouling* 22, 339–360. doi: 10.1080/08927010600980223

Gindl, M., Sinn, G., Gindl, W., Reiterer, A., and Tschegg, S. (2001). A comparison of different methods to calculate the surface free energy of wood using contact angle measurements. *Colloids Surf. A* 181, 279–287. doi: 10.1016/S0927-7757(00)00795-0

Haisch, C. (2012). Photoacoustic spectroscopy for analytical measurements. *Meas. Sci. Technol.* 23:17. doi: 10.1088/0957-0233/23/1/012001.

Herbert, S. K., Fork, D. C., and Malkin, S. (1990). Photoacoustic measurements *in vivo* of energy storage by cycling electron flow in algae and higher plants. *Plant Physiol.* 94, 926–934. doi: 10.1104/pp.94.3.926

Heydorn, A., Nielsen, A. T., Hentzer, M., Sternberg, C., Givskov, M., Ersbøll, B. K., et al. (2000). Quantification of biofilm structures by the novel computer program COMSTAT. *Microbiology* 146, 2395–2407. doi: 10.1099/00221287-146-10-2395

Inaba, T., Ichihara, T., Yawata, Y., Toyofuku, M., Uchiyama, H., and Nomura, N. (2013). Three-dimensional visualization of mixed species biofilm formation together with its substratum. *Microb. Immunol.* 57, 589–593. doi: 10.1111/1348-0421.12064

Ionescu, D., Siebert, C., Polerecky, L., Munwes, Y. Y., Lott, C., Häusler, S., et al. (2012). Microbial and chemical characterization of underwater fresh water springs in the . *PLoS ONE* 7:e38319. doi: 10.1371/journal.pone.0038319

Jones, P. R., Cottrel, M. T., Kirchman, D. L., and Dexter, S. C. (2007). Bacterial community structure of biofilms on artificial surfaces in an estuary. *Microb. Ecol.* 53, 153–162. doi: 10.1007/s00248-006-9154-5

Kautsky, L., and Kautsky, N. (2000). "The Baltic Sea, including Bothnian Sea and Bothnian Bay," in *Seas at the Millennium: an Environmental Evaluation,* ed C. R. R. Sheppard (Amsterdam: Elsevier Science Ltd.,), 121–133.

Kazemipour, F., Meleder, V., and Launeau, P. (2011). Optical properties of microphytobenthic biofilms (MPBOM): biomass retrieval implication. *J. Quant. Spectrosc. Radiat. Transf.* 112, 131–142. doi: 10.1016/j.jqsrt.2010.08.029

Klapper, I., and Dockey, J. (2010). Mathematical description of microbial biofilms. *SIAM Rev.* 52, 221–265. doi: 10.1137/080739720

Krishnan, S., Weinman, C. J., and Ober, C. K. (2008). Advances in polymers for anti-biofouling surfaces. *J. Mater. Chem.* 18, 3405–3413. doi: 10.1039/b801491d

Lakshmi, K., Muthukumar, T., Doble, M., Vedaprakash, L., Kruparathnam, C., Dineshram, R., et al. (2012). Influence of surface characteristics on biofouling formed on polymers exposed to coastal sea waters of India. *Colloids Surf. B* 91, 205–211. doi: 10.1016/j.colsurfb.2011.11.003

Lamprecht, M. R., Sabatini, D. M., and Carpenter, A. E. (2007). CellProfiler: free, versatile software for automated biological image analysis. *BioTechniques* 42, 71–75. doi: 10.2144/000112257

Lodhi, H. M. (2010). *Adavances in Computational Systems Biology*. New York, NY: John Wiley & Sons 1–17.

Mauzerall, D. C. (1990). Determination of oxygen emission and uptake in leaves by pulsed, time resolved photoacoustics. *Plant Physiol.* 94, 278–283. doi: 10.1104/pp.94.1.278

Mazurek, A., Pogorzelski, S. J., and Boniewicz-Szmyt, K. (2009). Adsorption of natural surfactants present in sea waters at surfaces of minerals: contact angle measurements. *Oceanologia* 51, 377–403. doi: 10.5697/oc.51-3.377

Mueller, L. N., de Brouwer, J. F. C., Almeida, J. S., Stal, L. J., and Xavier, J. B. (2006). Analysis of a marine phototrophic biofilm by confocal laser scanning microscopy using the new image quantification software PHLIP. *BMC Ecol.* 6:1. doi: 10.1186/1472-6785-6-1

Picioreanu, C., van Loosdrecht, M. C., and Heijnen, J. J. (1998). Two-dimensional model of biofilm detachment caused by internal stress from liquid flow. *Biotech. Bioeng.* 72, 205–218. doi: 10.1002/1097-0290(20000120)72:2<205::AID-BIT9>3.0.CO;2-L

Pinchasov, Y., Kotliarevsky, D., Dubinsky, Z., Mauzerall, D. C., and Feitelson, J. (2005). Photoacoustics as a diagnostic tool for probing the physiological status of phytoplankton. *Isreael J. Plant Sci.* 53, 1–10. doi: 10.1560/4DVV-JT78-G7VW-QTFM

Pinchasov, Y., Porat, R., Zur, B., and Dubinsky, Z. (2007). Photoacoustics: a novel tool for the determination of photosynthetic energy storage efficiency in phytoplankton. *Hydrobiologia* 579, 251–256. doi: 10.1007/s10750-006-0408-5

Pogorzelski, S. J., Mazurek, A. Z., and Szczepanska, A. (2013). *In-situ* surface wettability parameters of submerged in brackish water surfaces derived from captive bubble contact angle studies as indicators of surface condition level. *J. Mar. Syst.* 119–120, 50–60. doi: 10.1016/j.jmarsys.2013.03.011

Pogorzelski, S. J., Rochowski, P., and Szurkowski, J. (2014). *Pinus sylvestris* L. needle surface wettability parameters as indicators of atmospheric environment pollution impacts: novel contact angle hysteresis methodology. *Appl. Surf. Sci.* 292, 857– 866. doi: 10.1016/j.apsusc.2013.12.062

Pogorzelski, S. J., and Szczepanska, A. (2014). On-line and *in-situ* kinetics studies of biofilm formation on solid marine submerged substrata by contact angle wettability and microscopic techniques, IEEE Conference Publications, Baltic International Symposium (BALTIC), 2014 IEEE/OES, IEEE *Xplore*, 1–8.

Poulet, P., Cohen, D., and Malkin, S. (1983). Photoacoustic detection of photosynthetic oxygen evolution from leaves. Quantitative analysis by phase and amplitude measurements. *Biochim. Biophys. Acta* 724, 433–446. doi: 10.1016/0005-2728(83)90104-4

Railkin, A. (2004). *Marine Biofouling: Colonization Processes and Defenses*. Boca Raton, FL: CRC Press 25–31.

Rosencwaig, A. (1980). *Photoacoustics and Photoacoustic Spectroscopy,* New York, NY: Wiley Interscience Publication.

Rubio, C. (2002). These de l' Universite de Paris VI.

Schagerl, M., and Donabaum, K. (2003). Patterns of major photosynthetic pigments in freshwater algae. 1. Cyanoprokaryota, Rhodophyta and Cryptophyta. *Ann. Limnol.- Int. J. Lim.* 39, 35–47. doi: 10.1051/limn/2003003

Schagerl, M., Pichler, C., and Donabaum, K. (2003). Patterns of major photosynthetic pigments in freshwater algae. 2. Dinophyta, Euglenophyta, Chlorophyceae and Charales. *Ann. Limnol.- Int. J. Lim.* 39, 49–62. doi: 10.1051/limn/2003005

Schmid, T. (2006). Photoacoustic spectroscopy for process analysis. *Anal. Bioanal. Chem.* 384, 1071–1086. doi: 10.1007/s00216-005-3281-6

Schmidt, D. L., Brady, R. F., Lam, K., Schmidt, D. C., and Chaudhury, M. K. (2004). Contact angle hysteresis, adhesion, and marine biofouling. *Langmuir* 20, 2830–2836. doi: 10.1021/la035385o

Simões, M., Cieto, S., Pereira, M. O., and Viera, M. J. (2007). Influence of biofilm composition on the resistance to detachment. *Water Sci. Technol.* 55, 473–480. doi: 10.2166/wst.2007.293

Swearingen, M. C., Mehta, A., Mehta, A., Nistico, L., Hill, P. J., and Falzarano, A. R. (2016). A novel technique using potassium permanganate and reflectance confocal microscopy to image biofilm extracellular polymeric matrix reveals non-eDNA networks in Pseudomonas aeruginosa biofilms *FEMS Pathog. Dis.*74:ftv104. doi: 10.1093/femspd/ftv104

Szurkowski, J., Bańcik-Remisiewicz, A., Matusiak, K., and Tukaj, Z. (2001). Oxygen evolution and photosynthetic energy storage during the cell cycle of green alga *Scenedesmus armatus* characterized by photoacoustic spectroscopy. *J. Plant Physiol.* 158, 1061–1067. doi: 10.1078/0176-1617-00244

Szurkowski, J., Pawelska, I., Wartewig, S., and Pogorzelski, S. J. (2000). Photoacoustic study of the interaction between thin oil layers with water. *Acta Physica Polonica A* 97, 1073–1082. doi: 10.12693/APhysPolA.97.1073

Szurkowski, J., and Tukaj, Z. (1995). Characterization by photoacoustic spectroscopy of the photosynthetic *Scenedesmus armatus* system affected by fuel oil contamination. *Arch. Environ. Contam. Toxicol.* 29, 406–410. doi: 10.1007/BF00212508

Thomas, E., and Muirhead, D. (2009). Impact of wastewater fouling on contact angle. *Biofouling* 25, 445–454. doi: 10.1080/08927010902875105

Veeranjaneyulu, K., Charland, M., Charlebois, D., and Leblanc, R. M. (1991). Photosynthetic energy storage of Photosystem I and II in the spectral range of photosynthetically active radiation in intact sugar maple leaves. *Photosyn. Res.* 30, 131–138. doi: 10.1007/BF00042011

Wanner, O., Eberl, H., Morgenroth, E., Noguera, D., Picioreanu, C., Rittmann, B., et al. (2006). *Mathematical Modeling of Biofilms*, IWA Scientific and Technical Report No. 18, IWA Publishing, 36.

Yang, X., Beyenal, H., Harkin, G., and Lewandowski, Z. (2000). Quantifying biofilm structure using image analysis. *J. Microbiol. Methods* 39, 109–119. doi: 10.1016/S0167-7012(99)00097-4

Yawata, Y., Nguyen, J., Stocker, R., and Rusconi, R. (2016). Microfluidic studies of biofilm formation in dynamic environments. *J. Bacteriol.* 198, 2589–2595. doi: 10.1128/JB.00118-16

Zhao, Q., Liu, Y., Wang, C., Wang, S., and Muller-Steinhagen, H. (2005). Effect of surface free energy on the adhesion of biofouling and crystalline fouling. *Chem. Eng. Sci.* 60, 4858–4865. doi: 10.1016/j.ces.2005.04.006

Zwietering, M. H., Jongenburger, I., Romboust, F. M., and van 't Riet, K. (1990). Modeling of the bacterial growth curve. *Appl. Environ. Microbiol.* 56, 1875–1881.

Conflict of Interest Statement: The authors declare that the research was conducted in the absence of any commercial or financial relationships that could be construed as a potential conflict of interest.

The reviewer VD and handling editor declared their shared affiliation.